

ORIGINAL ARTICLE

# Element geochemical characteristics of a soil profile developed on dolostone in central Guizhou, southern China: implications for parent materials

Xingxing Cao<sup>1</sup> · Pan Wu<sup>1</sup> · Zhenxing Cao<sup>2</sup>

Received: 29 December 2015 / Revised: 6 June 2016 / Accepted: 6 July 2016 / Published online: 18 July 2016  
© Science Press, Institute of Geochemistry, CAS and Springer-Verlag Berlin Heidelberg 2016

**Abstract** This study presents bulk chemical compositions of the Tongmuling soil profile, which developed on dolostone, and the overlying strata covering the bedrock in the central Guizhou province (southern China). The chemical weathering characteristics of the studied profile were investigated and the inheritance relationships between the terra rossa and overlying strata were discussed. The results show that there is no remarkable variation in the major elements and weathering indices from the rock–soil interface to the topsoil, indicating that the studied profile was not typical for in situ crustal chemical weathering. The terra rossa were mainly composed of  $\text{SiO}_2$ ,  $\text{Al}_2\text{O}_3$  and  $\text{Fe}_2\text{O}_3$ . Compared with the insoluble residues and overlying strata, the terra rossa are characterized by an enrichment of Y and Cs and depletion of Ba and Sr. The subsoil shows a notable Ce negative anomaly, characterized by heavy rare earth element enrichment ( $L/H = 1.55\text{--}3.74$ ), whereas the topsoil shows a positive Ce anomaly with light rare earth element enrichment ( $L/H = 5.93\text{--}9.14$ ). According to Laterite-forming capacity estimates, the terra rossa could not have only been formed from acid-insoluble residues from the bedrock;  $\text{Al}_2\text{O}_3$  versus  $\text{Fe}_2\text{O}_3$  and Nb plotted against Ta show significant positive correlations between the terra rossa and overlying strata. The Eu/Eu\* versus

$\text{Gd}_\text{N}/\text{Yb}_\text{N}$  and ternary diagrams for Sc, Th, Zr, and Ta suggest that the overlying strata could also provide parent materials for the genesis of terra rossa.

**Keywords** Terra rossa · Dolomite · Parent materials · Guizhou · China

## 1 Introduction

Globally, karsts account for approximately 15 % of the land area (Jiang et al. 2009). Terra rossa, a type of reddish silty clay soil that forms on hard carbonate rocks, is widely distributed as a discontinuous layer ranging in thickness from a few centimeters to several meters in karst regions (Durn et al. 1999; Durn 2003; Merino et al. 2006). Because of the tremendous differences in chemical composition between terra rossa and the underlying carbonates, the identification of their parent materials has been debated over the past several decades. Currently, there are three main hypotheses: (1) terra rossa originates only from the underlying carbonates (Ahmad et al. 1966; Bronger et al. 1983; Ji et al. 2004a, b; Feng et al. 2009; Wei et al. 2013); (2) terra rossa genesis is affected by external materials, such as volcanic ash, non-carbonate rocks, and eolian dust (Olson et al. 1980; Durn et al. 1999; Delgado et al. 2003; Mee et al. 2004; Cooke et al. 2007; Durn et al. 2007; Muhs and Budahn 2009; Liu et al. 2013; Sandler et al. 2015); (3) terra rossa is formed by metasomatic replacement processes (Zhu and Li 2002; Merino and Banerjee 2008; Zhu et al. 2008; Lucke et al. 2014). These hypotheses are proposed for sites with different geologic and climatic settings all over the world.

The Guizhou Province is located in southwestern China, at the center of the East Asian karst zone, where carbonate terrains occupy more than 70 % of the land surface (Wu

---

**Electronic supplementary material** The online version of this article (doi:10.1007/s11631-016-0116-4) contains supplementary material, which is available to authorized users.

---

✉ Pan Wu  
pwu@gzu.edu.cn

<sup>1</sup> College of Resource and Environmental Engineering,  
Guizhou University, Guiyang 550025, Guizhou, China

<sup>2</sup> Graduate School of Science and Technology, Shizuoka  
University, Shizuoka 422-8529, Japan

et al. 2009). Previous studies indicated that the terra rossa of the Guizhou karst plateau may have resulted from in situ carbonate weathering (Wang et al. 1999; Ji et al. 2000, 2004a, b; Feng et al. 2009; Wei et al. 2013) rather than a metasomatic mechanism. However, the content of insoluble material in carbonates is very low. Approximately 1 % of acid insoluble residues were found in a previously studied profile (Ji et al. 2004a); this concentration is not sufficient to form the target profile. Hence, additional information regarding the parent materials of terra rossa in the Guizhou Province is still needed.

According to previous research, the underlying carbonates of this terra rossa were widely distributed in the Triassic, with additional deposition of other strata since the later Triassic (Team 1995). Therefore, the weathering of the strata covering the bedrock through time would be a possible source of terra rossa, and the weathering residues would not disappear without the action of a geological process. The purposes of this study are to investigate the major, trace and rare earth elemental variations of a terra rossa profile to determine if it is a product of in situ weathering, and to discuss the inherent relationship between the terra rossa and overlying strata. These results are relevant for the further study of terra rossa parent material in general.

## 2 Materials and methods

### 2.1 Geologic setting and geography

The Guizhou Province lies on the eastern Yunnan–Guizhou Plateau in southwestern China (Fig. 1a). It is part of the Yangtze Platform and contains mainly Proterozoic clastic sedimentary rocks and Paleozoic to Upper–Middle Triassic marine carbonate rocks; sediments deposited after the Triassic are mainly fluvial (Team 1995). The carbonate rocks in southwestern China form one of the largest continuous karst distributions in the world with an approximate area of 500,000 km<sup>2</sup> (Yuan 1992). In Guizhou Province, 109,000 km<sup>2</sup> of the land area is karst landscape.

The province has a subtropical monsoonal climate, in which most of the regions are mild and wet. The mean annual temperature is 8–12 °C, and the mean annual rainfall is 850–1600 mm. Approximately 50 % of the rainfall occurs from June to August. The study area is in central Guizhou Province (Fig. 1a). The major geological structure is the Guiyang syncline. The core of the syncline stratum is the Jurassic Ziliujing Formation, and the flank Formations (from youngest to oldest) are the Erqiao + Sanqiao, Yangliujing, Guanling, and Anshun (Fig. 1b). According to the stratigraphic relationship (Fig. 1c), the exposed Anshun Formation from the syncline wings could be associated with the weathering and erosion of the overlying strata.

## 2.2 Sampling and analytical methods

### 2.2.1 Profiles and sampling

The soil profiles were sampled in November 2008 at the Tongmuling Village (TML; 26°22'29"N, E 106°40'27"E; Fig. 1b), southwest of Guiyang, the capital of Guizhou Province. They formed on the Anshun Formation, which consists of early Triassic dolomites with approximately 0.68 % acid insoluble residues. The total thickness of the bedrock is 50–301 m (Fig. 1c). The sampling site lies at the top of a karst hill and contains an 8-m-thick terra rossa (Fig. 2a). The soil layers covering the bedrock are discontinuous, and there is no obvious transition layer from bedrock to soil. Field observations (photos of field investigation are shown in supplementary material) found that at the weathering frontier, dolomite had weathered into powder and, through the actions of water and gravity, the terra rossa from the bottom of the TML profile infilled part of this powder (Fig. 2b). Before sampling, a pit was dug from which the soil samples (TML4–19) were collected from the bottom to the top of the profile at a 50-cm resolution. Bedrock (TML1), cataclastic dolomite (TML2) and dolomite powder (TML3) were also collected. The overlying strata from the Triassic Guanling (T<sub>2</sub>g) and Yangliujing (T<sub>2</sub>yl) Formations were sampled, and seven samples were collected from the Triassic Erqiao + Sanqiao (CR1) and Jurassic Ziliujing clastic rock (CR2–7) Formations.

### 2.2.2 Experimental and chemical analysis methods

After air-drying, the rock and soil samples were ground (200 mesh) by a ceramic mortar and pestle. The method to extract insoluble residues from dolomites was described in detail by Wang et al. (1999). Soil organic matter was measured using the potassium dichromate volumetric method (NY/T 1121.6-2006). Values of pH were determined from a mixture of soil to CO<sub>2</sub>-free pure water (1:2.5) with a pH analyzer (HORIBA). Major element concentrations were measured using X-ray fluorescence (XRF) spectrometry (Philips, PW2404), according to the GB/T14506.28-93 silicate rock chemical analytical procedure. The concentrations of trace and rare earth elements were analyzed using quadrupole inductively-coupled plasma mass spectrometry (Q-ICP-MS; PerkinElmer, ELAN DRC-e). Organic matter and pH data were determined at the College of Resource and Environmental Engineering at Guizhou University, while the terra rossa and bedrock major element data were provided by the Beijing Research Institute of Uranium Geology. The major elements of overlying strata and all trace elements were identified at the Institute of Geochemistry, Chinese Academy of Sciences.

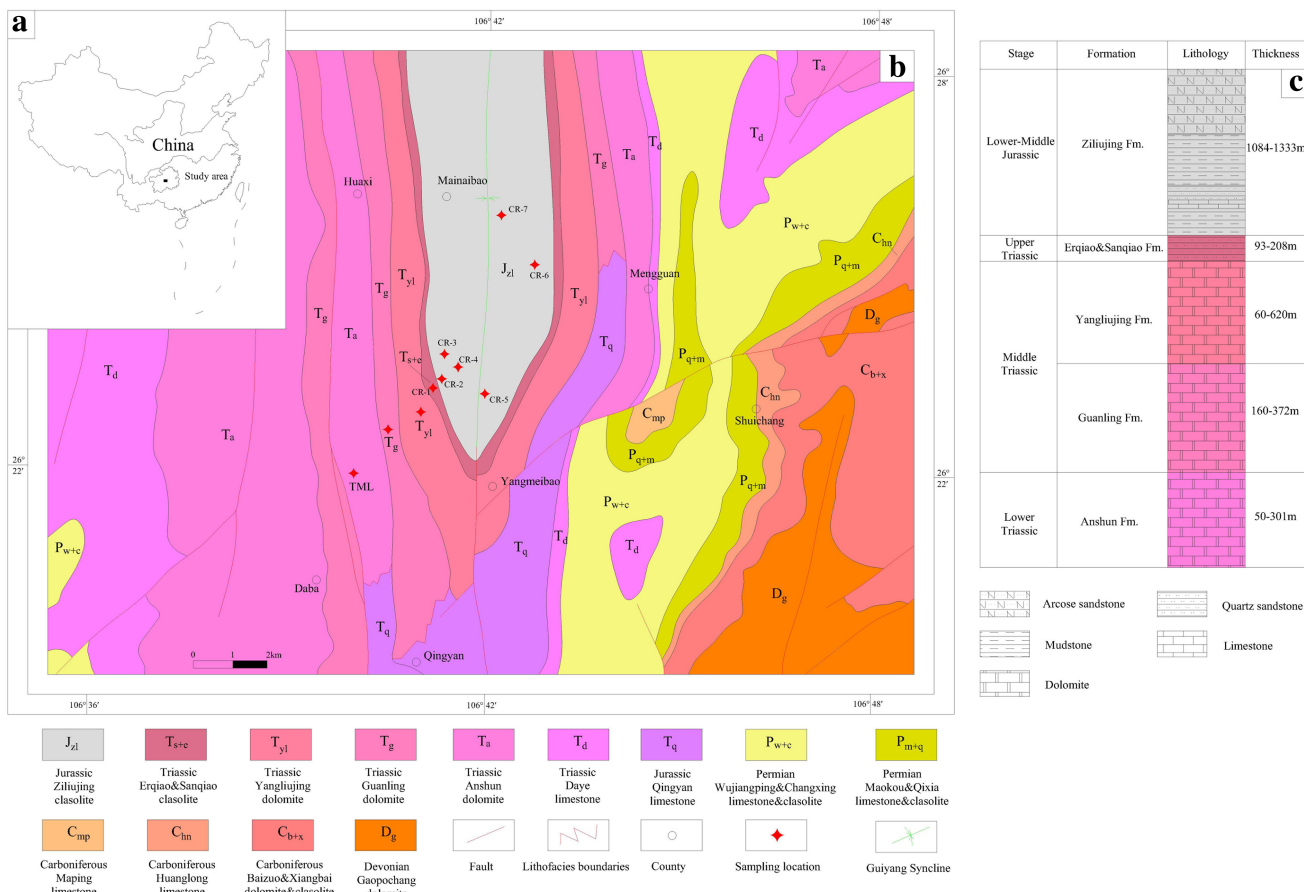


**Fig. 1** **a** Map showing the location of western Guizhou, China. **b** Geologic sketch of the study area and different lithologies. **c** Lithostratigraphic log above the Anshun Formation (modified from a 1:200,000 regional geological map, 1977)

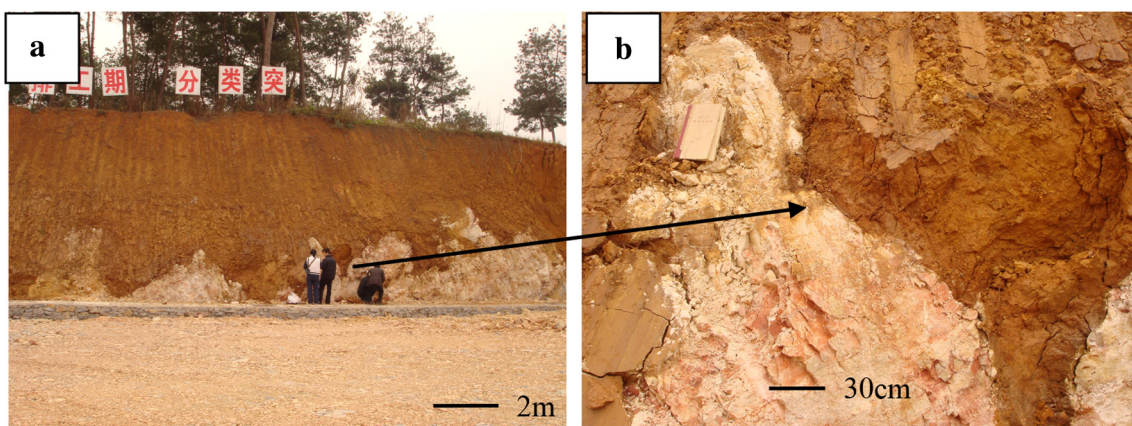


**Fig. 2** **a** Photos of the sampling profiles and **b** the rock–soil interface

### 3 Results

#### 3.1 Major element

The contents of the major elements in samples from the TML profile are listed in Table 1. The bedrock is mainly

composed of CaO and MgO, while Al<sub>2</sub>O<sub>3</sub>, SiO<sub>2</sub>, Fe<sub>2</sub>O<sub>3</sub> and loss-on-ignition (LOI) values account for 90 w%–97 w% of the total terra rossa, as well as acid insoluble residues from the bedrock. Other substances thus only account for a small proportion. Because the organic matter content is low, the high LOI of the samples suggests a significant

**Table 1** Major element contents and CIA value of bulk samples from the TML profile (w%)

Samples <sup>a</sup>	SiO <sub>2</sub>	Al <sub>2</sub> O <sub>3</sub>	Fe <sub>2</sub> O <sub>3</sub>	CaO	MgO	K <sub>2</sub> O	Na <sub>2</sub> O	MnO	TiO <sub>2</sub>	P <sub>2</sub> O <sub>5</sub>	LOI	Organic matter	Total	CIA <sup>b</sup>	pH
TML-19	42.48	26.62	10.70	0.34	1.15	2.52	0.54	0.05	0.56	0.23	14.62	1.47	101.28	86	4.90
TML-18	36.68	30.85	11.65	0.25	1.38	3.05	0.41	0.03	0.60	0.25	14.69	0.82	100.66	87	5.20
TML-17	35.30	31.22	11.60	0.28	1.31	2.73	0.44	0.03	0.57	0.25	16.16	0.88	100.77	88	5.20
TML-16	34.42	31.11	11.79	0.30	1.45	2.68	0.43	0.04	0.63	0.22	16.80	0.93	100.80	88	5.20
TML-15	34.65	26.68	11.27	0.28	1.38	3.02	0.46	0.06	0.50	0.20	21.58	0.60	100.68	85	5.40
TML-14	36.03	31.53	11.37	0.29	1.42	3.10	0.46	0.07	0.62	0.25	14.87	0.53	100.54	87	5.40
TML-13	35.04	30.42	11.90	0.29	1.35	2.83	0.42	0.07	0.59	0.26	16.65	0.35	100.17	88	5.40
TML-12	34.08	29.84	12.68	0.36	1.34	2.69	0.49	0.10	0.56	0.24	17.74	0.53	100.65	87	5.40
TML-11	34.36	31.00	11.67	0.33	1.33	2.72	0.53	0.08	0.57	0.26	17.30	0.33	100.48	88	5.30
TML-10	35.97	30.28	10.43	0.35	1.52	2.56	0.46	0.06	0.60	0.30	17.32	0.55	100.40	88	5.60
TML-9	35.66	31.60	10.05	0.26	1.35	2.57	0.42	0.10	0.60	0.26	17.24	0.73	100.84	89	5.50
TML-8	36.63	31.24	8.76	0.32	1.40	2.71	0.51	0.04	0.63	0.29	17.32	0.50	100.35	88	5.10
TML-7	32.70	29.62	12.71	0.25	1.25	2.21	0.39	0.04	0.58	0.23	19.83	0.38	100.19	89	5.20
TML-6	34.15	27.80	12.40	0.33	2.23	2.57	0.44	0.06	0.56	0.25	18.96	0.68	100.43	87	5.70
TML-5	33.76	29.38	11.95	0.48	1.48	2.44	0.62	0.08	0.60	0.25	18.74	1.09	100.87	87	7.00
TML-4	34.44	29.66	12.54	0.42	1.52	2.56	0.44	0.06	0.56	0.27	17.62	0.98	101.07	87	7.20
TML-3	1.14	0.10	0.42	30.86	21.49	0.18	0.45	–	0.05	0.05	45.08	0.04	99.86		
TML-2	0.54	0.10	0.40	32.10	21.29	0.19	0.62	–	0.05	0.05	44.77	0.03	100.14		
TML-1	0.70	0.10	0.43	30.40	21.66	0.15	0.43	–	0.05	0.05	45.86		99.83		
HX-1	55.92	19.96	3.67	0.69	2.11	4.92	0.65	0.01	1.25	0.05	10.71		99.94	72	

<sup>a</sup> TML-1, TML-2 and TML-3 stand for bedrock, cataclastic dolomite and dolomite powder, respectively. Sample HX-1 stand for the acid-insoluble residues from Anshun Formation dolomite. The symbol “–” means the content is under the test limit

<sup>b</sup> The chemical index of alteration (CIA) = Al<sub>2</sub>O<sub>3</sub>/(Al<sub>2</sub>O<sub>3</sub> + CaO\* + NaO + K<sub>2</sub>O), where CaO\* only represents the Ca in silicate (Nesbitt and Young 1982, 1989)

contribution from clay minerals. The TML profile shows only slight differences in chemical composition among the bedrock, cataclastic dolomite rock and rock powder, but the content of SiO<sub>2</sub> in TML3 is slightly higher than in TML1 and TML2, mainly as a result of the clay minerals in the overlying terra rossa. Table 1 shows that the pH increases with depth; thus, SiO<sub>2</sub> may have dissolved into Si(OH)<sub>4</sub> and migrated into the rock powder layer. The chemical index of alteration varies from 85 to 89, and there is no significant variation from the rock–soil interface to the top of the profile (Table 1).

### 3.2 Trace elements

The trace element contents are listed in Table 2. An average upper continental crust (UCC) normalized spider diagram of the samples from the studied profiles is shown in Fig. 3. The results show that the UCC-normalized trace element distribution patterns of the soil samples are quite similar as a whole, as characterized by the remarkable depletion of Sr and Ba relative to the UCC. The trace elements in the samples of bedrock and acid insoluble residues both show similar element distribution patterns,

except for Sr, Y and Ni. However, the trace element content in the potential parent materials is significantly different due to lithologic variability. All of the terra rossa samples have similar UCC-normalized spider diagrams to bedrock acid insoluble residues (HX-1) and potential parent materials, especially the residues from T<sub>2</sub>g and T<sub>2</sub>yl (T<sub>2</sub>g-1 and T<sub>2</sub>yl-1, respectively).

### 3.3 Rare earth elements

The concentrations and relevant parameters of rare earth elements (REEs) are listed in Table 3. The total REE contents ( $\Sigma$ REE) of the terra rossa samples varied considerably from 351.27 to 2225.31 ppm, and the  $\Sigma$ REE increased gradually with depth. The  $\Sigma$ REE in the underlying bedrock and their insoluble residues ranged from 8.06 to 133.93 ppm, whereas the  $\Sigma$ REE in the potential parent materials (CR1–7, T<sub>2</sub>g-1 and T<sub>2</sub>yl-1) ranged from 32.89 to 195.14 ppm. The terra rossa samples showed significant negative cerium (Ce) anomalies at the bottom of the studied profiles, and all of the samples showed negative europium (Eu) anomalies ranging from 0.48 to 0.75.

**Table 2** Trace element contents of bulk samples from the profile and overlying strata

Samples <sup>a</sup>	TML-1	TML-2	TML-3	TML-4	TML-5	TML-6	TML-7	TML-8	TML-9	TML-10	
Sc	0.17	0.18	0.45	30.10	36.60	32.10	28.20	24.80	32.80	30.50	
V	7.36	6.71	11.00	327.00	303.00	329.00	334.00	283.00	302.00	300.00	
Cr	5.53	8.31	6.84	138.00	119.00	123.00	124.00	117.00	117.00	115.00	
Co	0.80	0.85	1.35	29.70	31.40	30.50	23.20	21.00	38.10	29.90	
Ni	7.82	11.10	10.10	106.00	187.00	107.00	96.90	101.00	122.00	113.00	
Cu	2.46	3.94	4.59	95.62	93.18	87.86	99.61	91.29	107.16	98.39	
Zn	8.34	13.30	12.70	253.00	271.00	251.00	250.00	247.00	283.00	274.00	
Ga	0.34	0.36	1.14	41.20	40.90	38.80	40.10	37.30	41.80	39.00	
Rb	1.78	1.86	4.55	155.00	159.00	154.00	142.00	149.00	152.00	150.00	
Sr	77.80	81.90	73.90	48.40	55.10	54.40	51.20	51.90	54.40	57.60	
Y	12.50	10.50	36.00	371.00	1090.00	200.00	224.00	217.00	197.00	140.00	
Zr	2.48	2.33	6.03	188.00	195.00	201.00	196.00	194.00	200.00	200.00	
Nb	0.31	0.28	0.66	21.00	23.40	23.70	22.20	22.10	22.90	23.80	
Cs	0.12	0.09	0.43	21.90	22.60	23.40	24.00	24.00	24.60	23.70	
Ba	3.97	5.94	8.91	234.00	330.00	242.00	196.00	220.00	225.00	228.00	
Hf	0.08	0.11	0.22	5.69	7.42	5.92	5.68	5.80	6.03	5.80	
Ta	0.04	0.05	0.07	1.47	1.85	1.71	1.57	1.68	1.68	1.72	
W	0.15	0.15	0.20	3.61	4.40	6.33	3.77	3.97	3.97	4.03	
Pb	1.51	2.46	3.15	84.36	114.39	91.73	75.78	72.04	122.09	101.96	
Th	0.23	0.26	0.73	26.10	26.00	27.60	28.10	25.80	30.80	28.00	
U	0.57	0.60	0.47	6.08	6.90	7.30	7.99	6.96	8.20	7.67	
Samples <sup>a</sup>	TML-11	TML-12	TML-13	TML-14	TML-15	TML-16	TML-17	TML-18	TML-19	HX-1 <sup>b</sup>	
Sc	37.00	31.60	29.00	29.80	27.10	25.00	28.10	28.50	26.10	12.00	
V	318.00	303.00	304.00	289.00	298.00	307.00	298.00	290.00	272.00	172.00	
Cr	117.00	122.00	118.00	114.00	118.00	121.00	131.00	128.00	117.00	74.40	
Co	32.30	41.20	35.00	40.60	43.10	32.80	38.50	22.30	26.00	7.53	
Ni	109.00	93.50	100.00	105.00	93.60	92.30	97.00	80.10	73.00	23.30	
Cu	108.04	81.50	82.10	83.50	84.20	81.90	81.30	77.10	68.00	37.83	
Zn	273.00	230.00	242.00	241.00	233.00	236.00	239.00	221.00	201.00	58.70	
Ga	40.60	39.00	37.70	38.20	37.70	37.50	38.20	38.70	34.20	27.40	
Rb	156.00	146.00	145.00	149.00	151.00	140.00	146.00	151.00	143.00	168.00	
Sr	53.90	57.30	58.80	59.20	58.80	58.00	59.10	67.90	69.10	93.80	
Y	118.00	95.60	91.50	82.10	82.10	77.60	79.50	67.10	49.00	17.60	
Zr	206.00	218.00	222.00	228.00	225.00	221.00	237.00	288.00	351.00	274.00	
Nb	23.40	25.50	25.10	24.90	25.40	25.30	27.20	32.00	34.70	30.20	
Cs	23.80	22.80	23.10	22.00	22.30	24.10	23.40	22.70	21.00	9.33	
Ba	217.00	228.00	225.00	229.00	236.00	232.00	233.00	258.00	275.00	403.00	
Hf	5.92	5.98	6.04	6.50	6.38	6.41	6.93	8.34	10.10	7.16	
Ta	1.62	2.00	1.84	1.83	1.86	1.89	1.97	2.31	2.56	1.97	
W	7.26	5.28	5.42	4.14	4.34	4.86	4.74	5.36	5.60	4.95	
Pb	102.29	101.13	101.79	107.61	103.55	89.59	96.29	82.00	77.82	29.48	
Th	30.10	28.30	29.10	29.50	28.80	30.80	31.10	31.70	30.60	9.77	
U	8.52	7.88	7.95	7.48	7.41	7.62	8.20	8.96	8.63	7.82	
CR-1 <sup>c</sup>	CR-2	CR-3	CR-4	CR-5	CR-6	CR-7	T <sub>2y</sub> l <sup>d</sup>	T <sub>2g</sub>	T <sub>2g</sub> -1 <sup>e</sup>	T <sub>2yl</sub> -1	
Sc	–	11.10	10.90	1.50	12.70	8.91	–	21.80	–	11.20	6.18
V	31.10	122.00	117.00	50.80	115.00	89.10	14.90	117.00	3.15	183.00	71.70
Cr	21.10	74.10	77.30	42.90	85.10	63.60	9.35	32.48	–	82.65	48.72

**Table 2** continued

	CR-1 <sup>c</sup>	CR-2	CR-3	CR-4	CR-5	CR-6	CR-7	T <sub>2yl</sub> <sup>d</sup>	T <sub>2g</sub>	T <sub>2g-1</sub> <sup>e</sup>	T <sub>2yl-1</sub>
Co	1.35	16.00	7.34	1.55	16.00	13.60	2.35	11.30	0.84	10.40	4.36
Ni	8.53	37.60	34.90	3.78	39.00	33.70	2.30	5.26	7.58	53.71	22.08
Cu	7.16	25.80	28.70	7.70	28.00	24.90	4.76	9.19	3.59	66.40	24.30
Zn	31.20	94.90	94.60	24.10	86.50	95.10	62.80	75.00	5.25	214.00	55.00
Ga	6.49	20.00	20.60	6.33	22.20	16.80	1.66	17.20	–	23.80	17.20
Rb	85.30	133.00	191.00	14.30	107.00	116.00	4.63	105.00	0.54	155.00	130.00
Sr	19.80	152.00	49.20	50.00	45.80	114.00	7.21	270.00	232.00	114.00	53.40
Y	12.10	25.80	28.40	17.70	42.20	27.40	6.11	22.10	0.47	8.51	8.81
Zr	136.00	127.00	159.00	206.00	202.00	179.00	148.00	91.90	1.09	212.00	263.00
Nb	5.02	15.00	16.00	8.18	16.70	13.70	2.86	9.63	0.11	22.70	16.70
Cs	2.51	12.20	15.60	0.87	11.10	8.19	0.35	10.80	0.05	15.50	11.10
Ba	138.00	388.00	290.00	55.90	224.00	304.00	24.10	626.00	2.34	221.00	187.00
Hf	3.01	3.12	3.91	4.69	4.95	4.34	3.16	2.66	0.02	5.94	6.76
Ta	0.41	1.31	1.30	0.62	1.36	1.08	0.21	0.54	0.06	1.15	0.97
W	0.85	2.46	2.48	1.07	2.53	2.00	0.49	0.41	0.27	3.74	2.82
Pb	10.49	33.34	24.37	18.19	29.46	22.19	4.32	22.00	0.96	58.30	15.90
Th	5.38	13.50	13.70	7.95	14.20	11.60	2.10	8.63	0.12	3.89	8.04
U	1.20	2.65	3.27	1.31	2.47	2.60	0.56	2.51	0.86	11.10	5.32

<sup>a</sup> TML-1, TML-2 and TML-3 stand for bedrock, cataclastic dolomite and dolomite powder, respectively. All the trace element values are in ppm

<sup>b</sup> Sample HX-1 stand for the acid-insoluble residues from Anshun Formation dolomite. The symbol “–” indicates that the content is under the test limit

<sup>c</sup> CR-1 to CR-7 stand for the clastic rock collected from the Erqiao + Sanqiao and Ziliujing Formations

<sup>d</sup> T<sub>2yl</sub> and T<sub>2g</sub> stand for the Yangliujing and Guanling Formation carbonate rocks, respectively

<sup>e</sup> T<sub>2yl-1</sub> and T<sub>2g-1</sub> stand for the acid-insoluble residues from samples T<sub>2yl</sub> and T<sub>2g</sub>, respectively

## 4 Discussion

### 4.1 The chemical weathering characteristics of the studied profile and its implications

#### 4.1.1 Major element geochemical ratios and characteristics

In the transformation from dolomite to an insoluble residue (HX-1), the content of less mobile elements, such as Al, Fe and Ti, increased, while the concentrations of mobile elements, such as Mg and Ca, decreased (Table 1). If the terra rossa had developed only from the insoluble residues of the dolomite bedrock, then with the leaching of Ca and Mg, the content of TiO<sub>2</sub> in it should be higher than the HX-1. However, the opposite result was observed (Table 1), which is consistent with a previous study of the Pingba (PB) profile (Ji et al. 2004a). These results indicate that external materials with a low TiO<sub>2</sub> concentration likely contribute to the genesis of the terra rossa.

The saltfemic rate (saf value) and base leaching degree are two indices that reflect the weathering degree of crust

(Huang 1996; Cui et al. 2001). The highest base leaching degree and the lowest saf value in the sequence indicate the highest resistance to weathering. The calculated results (Fig. 4) show that the saf values of the terra rossa are between 0.77 and 1.14 (mean 0.86), whereas the base leaching degree varies between 4.99 and 7.22 (mean 6.13). These results indicate that the TML profile underwent intense chemical weathering. For in situ crustal weathering, changes in the two indices should show a gradient. However, there is no obvious gradient in the whole profile and the change from bedrock to soil is distinct (Fig. 4), which is consistent with the PB profile (Ji et al. 2004a). As the TML and PB developed on the same strata (Anshun Formation) and the saf values of the rock powder samples (TML3 and Y3) were relatively higher (Fig. 4), it could be that the terra rossa in-filled part of the rock powder. This type of change would be consistent with field investigations (Fig. 2b).

Ternary diagrams (A-CN-K) portray the molar proportions of Al<sub>2</sub>O<sub>3</sub> (A apex), CaO + NaO (CN apex) and K<sub>2</sub>O (K apex) for bulk samples (Fig. 5) and are generally used to explain the degree of weathering and to predict the

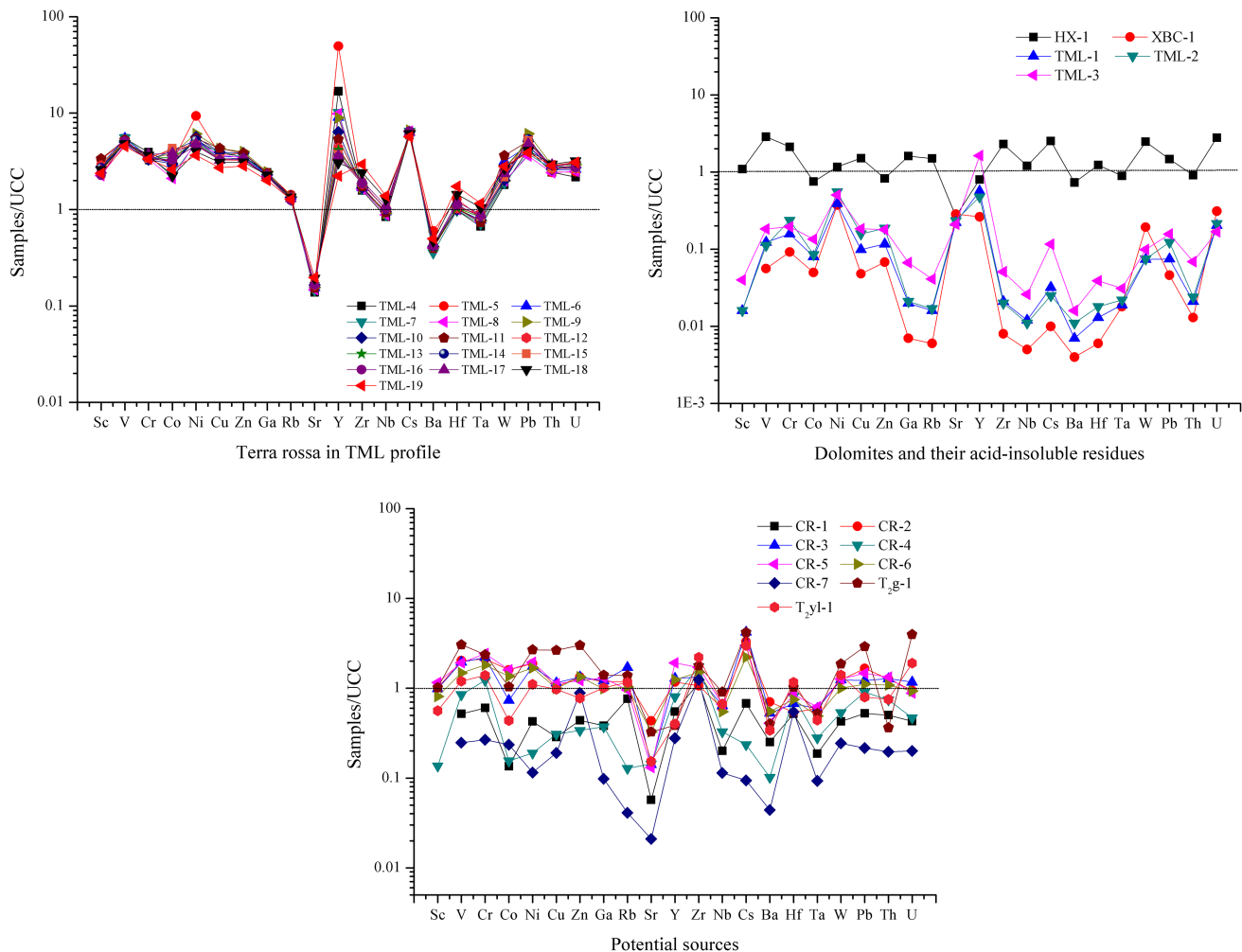


**Fig. 3** The upper continental crust (UCC)-normalized spider diagrams of terra rossa samples, underlying dolomite and their acid insoluble residues, and the overlying strata. The UCC data were obtained from Taylor and McLennan (1985)

continental chemical weathering trend (Nesbitt and Young 1989). The primary rock is plotted at the CN apex (Fig. 5), but the terra rossa samples cannot be notably distinguished and almost all of the samples clustered at the A apex. The dolomite weathered crust described in Ji et al. (2000) showed that the terra rossa plotted with increasing proximity to A from the lower part to the upper part of the profile, but this characteristic was not noticed in the TML profile (Fig. 5). According to previous research, the HX (Sun et al. 2002b) and PB (Ji et al. 2004a) profiles suggested that the acid insoluble residues from the bedrock powder (YT-3, HYF-1) plot between the acid insoluble residues from the bedrock and terra rossa, reflecting mixed characteristics. The plots of YT-3 and HYF-1 were closer to the terra rossa, and the base of the terra rossa showed a lower weathering intensity in the HX and PB profiles. This part of the soil may thus have mixed with the acid insoluble residues. All of the samples are distributed along the joint

A-K line, indicating that with the leaching of  $K_2O$ , the acid insoluble residues mixed into the terra rossa, gradually weathering the soil. Therefore, these results indicate that the TML profile does not have the typical characteristics of in situ crustal weathering.

Generally, Al/Ti remains relatively constant during weathering (Rye and Holland 1998; Young and Nesbitt 1998) and can be used to clearly distinguish the parent material of a terra rossa (Muhs et al. 1990; Ji et al. 2004a). Thus, the Al/Ti in the terra rossa divided by the same ratio in the bedrock should be close to 1, if it is an in situ weathering profile (Fig. 6). While the Huaxi (HX) (Sun et al. 2002b), Jishou (JS) (Wang et al. 2002), Longdongbao (LDB) (Zhou et al. 2005) and Xinpu (XP) (Ji et al. 2000) profiles were close to 1, consistent with an insoluble residue content from the bedrock  $\geq 3\%$ , the Guiyang (GY) (Li et al. 1991), PB (Ji et al. 2004a) and TML profiles, overlying the Anshun Formation, were slightly different. The

**Table 3** Rare earth element contents and relative parameters of bulk samples from the profile and overlying strata

Samples <sup>a</sup>	TML-1	TML-2	TML-3	TML-4	TML-5	TML-6	TML-7	TML-8	TML-9	TML-10
La	1.67	4.41	11.60	123.00	210.00	100.00	130.00	116.00	114.00	92.50
Ce	1.46	1.43	3.32	92.10	179.00	142.00	100.00	139.00	396.00	269.00
Pr	0.42	1.78	4.61	49.40	113.00	33.20	43.10	40.30	36.10	26.90
Nd	2.03	8.54	22.20	230.00	577.00	148.00	191.00	178.00	160.00	111.00
Sm	0.38	2.17	5.60	68.40	222.00	37.10	45.80	44.30	37.40	25.40
Eu	0.10	0.42	1.19	14.79	53.25	7.75	9.44	9.13	7.94	5.08
Gd	0.56	2.14	6.12	65.37	246.65	36.18	42.41	41.60	37.29	24.35
Tb	0.09	0.29	0.85	10.70	44.50	6.16	6.96	7.13	6.21	4.28
Dy	0.56	1.36	4.40	57.70	249.00	34.40	38.10	39.30	34.30	24.40
Ho	0.14	0.28	0.95	12.40	53.10	7.52	8.17	8.47	7.49	5.29
Er	0.39	0.59	2.21	31.50	135.00	19.00	20.90	22.00	19.80	13.80
Tm	0.04	0.06	0.22	4.11	18.30	2.63	2.82	3.04	2.71	1.93
Yb	0.20	0.32	1.15	24.90	109.00	16.30	17.00	18.20	16.60	11.90
Lu	0.03	0.05	0.16	3.62	15.50	2.33	2.50	2.65	2.35	1.70
LREE <sup>b</sup>	6.06	18.75	48.52	577.69	1354.25	468.05	519.34	526.73	751.44	529.88
HREE	1.99	5.09	16.06	210.30	871.05	124.52	138.86	142.39	126.75	87.65
L/H	3.04	3.69	3.02	2.75	1.55	3.76	3.74	3.70	5.93	6.05
ΣREE	8.06	23.83	64.59	787.99	2225.31	592.57	658.20	669.12	878.20	617.53
δCe	0.42	0.12	0.11	0.28	0.28	0.59	0.32	0.49	1.49	1.30
δEu	0.64	0.59	0.62	0.68	0.70	0.65	0.65	0.65	0.65	0.63
(La/Yb) <sub>N</sub>	5.74	9.44	6.80	3.33	1.30	4.14	5.16	4.30	4.63	5.24
(La/Sm) <sub>N</sub>	1.04	0.48	0.49	0.43	0.22	0.64	0.67	0.62	0.72	0.86
(Gd/Yb) <sub>N</sub>	2.29	5.47	4.30	2.12	1.83	1.79	2.01	1.84	1.81	1.65
Samples <sup>a</sup>	TML-11	TML-12	TML-13	TML-14	TML-15	TML-16	TML-17	TML-18	TML-19	HX-1 <sup>c</sup>
La	91.50	80.30	82.50	75.20	77.40	85.50	90.40	82.20	68.90	35.40
Ce	226.00	198.00	222.00	241.00	198.00	185.00	213.00	206.00	164.00	59.30
Pr	24.70	21.40	21.40	19.80	19.80	21.10	21.70	19.00	15.30	6.04
Nd	99.50	86.50	85.30	78.70	80.90	84.30	86.50	72.70	55.70	19.90
Sm	22.70	18.50	18.70	17.20	16.80	17.00	17.80	14.30	10.70	3.00
Eu	4.58	3.65	3.60	3.35	3.30	3.27	3.39	2.69	2.01	0.50
Gd	20.88	16.84	16.69	16.52	15.63	15.34	16.36	13.02	9.50	2.31
Tb	3.59	2.85	2.82	2.61	2.58	2.61	2.74	2.15	1.59	0.40
Dy	19.90	15.70	15.40	14.30	14.20	14.00	14.80	11.90	8.98	2.30
Ho	4.40	3.35	3.36	3.14	3.06	3.11	3.17	2.64	1.97	0.54
Er	11.40	9.03	8.73	8.41	8.29	8.43	8.65	7.38	5.55	1.70
Tm	1.59	1.28	1.20	1.18	1.16	1.18	1.22	1.08	0.84	0.26
Yb	9.77	7.94	7.58	8.36	7.36	7.29	7.94	6.60	5.40	1.98
Lu	1.42	1.18	1.11	1.08	1.17	1.17	1.12	1.00	0.83	0.30
LREE <sup>b</sup>	468.98	408.35	433.50	435.25	396.20	396.17	432.79	396.89	316.61	124.14
HREE	72.95	58.17	56.89	55.60	53.45	53.13	56.00	45.77	34.65	9.79
L/H	6.43	7.02	7.62	7.83	7.41	7.46	7.73	8.67	9.14	12.69
ΣREE	541.93	466.52	490.39	490.85	449.65	449.30	488.80	442.66	351.27	133.93
δCe	1.14	1.15	1.27	1.50	1.22	1.05	1.16	1.25	1.22	0.98
δEu	0.64	0.63	0.62	0.61	0.62	0.62	0.61	0.60	0.61	0.58
(La/Yb) <sub>N</sub>	6.31	6.82	7.34	6.06	7.09	7.91	7.68	8.40	8.60	12.05
(La/Sm) <sub>N</sub>	0.96	1.03	1.05	1.04	1.09	1.19	1.20	1.36	1.53	2.80
(Gd/Yb) <sub>N</sub>	1.72	1.71	1.78	1.59	1.71	1.70	1.66	1.59	1.42	0.94

**Table 3** continued

	CR-1 <sup>d</sup>	CR-2	CR-3	CR-4	CR-5	CR-6	CR-7	T <sub>2yl</sub> <sup>e</sup>	T <sub>2g</sub>	T <sub>2g-1</sub> <sup>f</sup>	T <sub>2yl-1</sub>
La	13.40	36.40	40.70	24.00	47.20	32.80	7.03	20.60	0.27	13.90	28.60
Ce	28.56	73.86	74.22	41.43	68.05	68.13	14.01	40.80	0.52	23.40	50.40
Pr	3.25	8.07	8.27	4.57	10.30	7.35	1.54	4.89	0.06	2.24	5.14
Nd	12.10	29.20	28.40	15.80	38.30	27.20	5.59	18.80	0.25	7.50	16.30
Sm	2.35	5.52	5.08	3.16	7.22	5.27	1.13	4.33	0.05	1.21	2.60
Eu	0.47	1.22	1.01	0.64	1.55	1.17	0.18	1.04	0.01	0.25	0.36
Gd	1.81	4.95	4.35	3.00	6.57	4.79	0.89	4.30	0.07	1.13	2.03
Tb	0.32	0.80	0.74	0.50	1.10	0.82	0.16	0.69	0.01	0.18	0.29
Dy	1.75	4.24	4.25	2.77	5.90	4.39	0.86	3.97	0.05	1.14	1.46
Ho	0.40	0.95	0.97	0.60	1.31	0.99	0.21	0.78	0.01	0.28	0.32
Er	1.09	2.52	2.68	1.63	3.56	2.65	0.56	2.31	0.04	1.00	1.05
Tm	0.16	0.36	0.40	0.24	0.49	0.38	0.09	0.33	0.005	0.15	0.17
Yb	1.10	2.39	2.58	1.58	3.13	2.46	0.56	2.20	0.03	1.21	1.30
Lu	0.15	0.36	0.38	0.25	0.47	0.36	0.08	0.32	0.005	0.19	0.20
LREE <sup>b</sup>	60.12	154.27	157.68	89.59	172.61	141.92	29.49	90.46	1.15	48.50	103.40
HREE	6.78	16.57	16.35	10.56	22.53	16.84	3.40	14.90	0.22	5.28	6.82
L/H	8.87	9.31	9.64	8.49	7.66	8.43	8.67	6.07	5.25	9.18	15.16
ΣREE	66.90	170.84	174.03	100.15	195.14	158.76	32.89	105.35	1.37	53.79	110.22
δCe	1.04	1.04	0.97	0.95	0.74	1.06	1.03	0.98	0.98	1.01	1.00
δEu	0.69	0.71	0.66	0.63	0.69	0.71	0.56	0.73	0.51	0.67	0.48
(La/Yb) <sub>N</sub>	8.21	10.27	10.64	10.24	10.17	8.99	8.40	6.31	5.46	7.74	14.83
(La/Sm) <sub>N</sub>	1.35	1.56	1.90	1.80	1.55	1.48	1.48	1.13	1.31	2.72	2.61
(Gd/Yb) <sub>N</sub>	1.33	1.67	1.36	1.53	1.69	1.57	1.27	1.58	1.73	0.75	1.26

<sup>a</sup> TML-1, TML-2 and TML-3 stand for bedrock, cataclastic dolomite and dolomite powder, respectively. All the rare earth element values are in ppm

<sup>b</sup> LREE and HREE represent La to Eu and Gd to Lu, respectively. L/H represents the concentration ratio of LREE and HREE.  $\sum \text{REE}$  = the sum of La to Lu,  $\delta\text{Ce} = \text{Ce}_N / (\text{Ce}_N \times \text{Pr}_N)^{0.5}$ ,  $\delta\text{Eu} = \text{Eu}_N / (\text{Eu}_N \times \text{Gd}_N)^{0.5}$ , (La/Sm)<sub>N</sub>, (Gd/Yb)<sub>N</sub> and (La/Yb)<sub>N</sub>, where N refers to a chondrite-normalized value (Boynton 1984)

<sup>c</sup> Sample HX-1 stand for the acid-insoluble residues from Anshun Formation dolomite

<sup>d</sup> CR-1 to CR-7 stand for the clastic rock collected from the Erqiao + Sanqiao and Ziliujing Formations

<sup>e</sup> T<sub>2yl</sub> and T<sub>2g</sub> represent the Yangliujing and Guanling Formation carbonate rocks, respectively

<sup>f</sup> T<sub>2yl-1</sub> and T<sub>2g-1</sub> denote the acid-insoluble residues from samples T<sub>2yl</sub> and T<sub>2g</sub>, respectively

ratio from the PB and TML profiles were greater than 1, but the GY profile was close to 1, despite the fact it overlayed the same Formation, suggesting that the terra rossa parent material was complex. For the profiles with ratios close to 1, the parent materials of the terra rossa may not be fully provided by the underlying bedrock. The source material may, instead, come from other areas, so that after the weathering residue covered the bedrock, the acid insoluble residue mixed with it in a late soil-forming process. Thus, a higher acid insoluble residue content means that more of underlying bedrock is retained in the soil, pushing the ratio close to 1. If the carbonate rocks are purer, there is a lower content of insoluble residue available to contribute to the formation of terra rossa.

#### 4.1.2 Trace element geochemical and fractionation characteristics

When the particular geochemical characteristics of the parent materials remain in the terra rossa, the distribution patterns of the trace elements and REEs can be used to trace the provenance of the weathering products (Wei et al. 2013). The spider diagram (Fig. 3) shows that the terra rossa from the TML profile has a similar trace element distribution, suggesting that the material in the studied profile has the same provenance. The UCC-normalized spider diagram of the terra rossa is not only similar to that of the bedrock acid insoluble residues (HX-1), but also shows similar element distribution patterns with potential parent materials, especially acid insoluble residues T<sub>2g-1</sub> and T<sub>2yl-1</sub>.

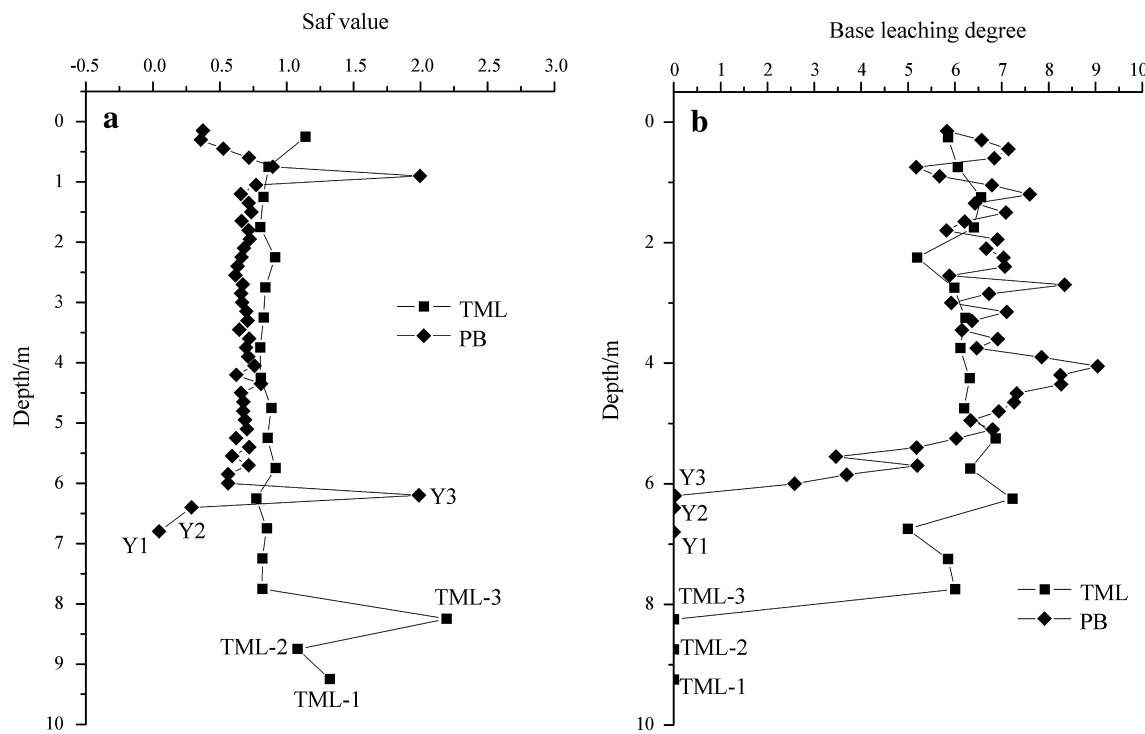


**Fig. 4** Variations in the chemical weathering intensity indices with depth in the TML profile. Base leaching degree =  $\text{Al}_2\text{O}_3/(\text{Na}_2\text{O} + \text{K}_2\text{O} + \text{CaO} + \text{MgO})$ , saf =  $\text{SiO}_2/(\text{Al}_2\text{O}_3 + \text{Fe}_2\text{O}_3)$ . Y1, Y2 and Y3 are dolomite, weathered dolomite and dolomite powder, respectively. The Pingba (PB) data used here are from Ji et al. (2004a)

Compared with the acid insoluble residues and potential parent materials, the samples from the terra rossa are characterized by an enrichment of Y and Cs and a depletion of Ba and Sr (Fig. 3). Barium has long been known to exhibit different weathering behavior than other, more mobile alkaline earth elements (Nesbitt et al. 1980; Buggle et al. 2011). In contrast, the ionic potential of  $\text{Sr}^{2+}$  (1.8) closely mimics that of  $\text{Ca}^{2+}$  (2.0) (Panahi et al. 2000) and is easily substituted for Ca in calcium carbonate (Plank and Langmuir 1998); therefore, Sr is rapidly removed (as a dissolved species) during weathering (Nesbitt et al. 1980). Alkali elements (K, Rb, Cs) were the first main group elements and dominant in the K-feldspars, illite and kaolinite (Plank and Langmuir 1998); they show similar behavior in the weathering profile, which is influenced by the solubility of the host minerals of K-feldspar or illite. However, yttrium (Y) is concentrated in the clay-rich portion of the weathering profile (Nesbitt and Markovics 1997; Hill et al. 2000; Panahi et al. 2000), leading to the unusual enrichment of Y in the studied profile.

#### 4.1.3 REE geochemical and fractionation characteristics

Figure 7 shows the REE distribution patterns in the TML profile. The normalized patterns reveal that the terra rossa samples show different REE distribution patterns than

expected for the same Eu anomalies. The bottom soil shows a notable negative Ce anomaly, characterized by heavy (H) REE enrichment ( $L/H = 1.55\text{--}3.74$ ), whereas the top of the profile shows a positive Ce anomaly with light (L) REE enrichment ( $L/H = 5.93\text{--}9.14$ ).

It is generally believed that the lower mobility of LREE compared to HREE causes LREE enrichment in the upper section of weathered crust and the HREE enrichment in the bottom (Nesbitt 1979; Duddy 1980). While REEs have a particularly stable  $3^+$  oxidation state (Laveuf and Cornu 2009), Eu and Ce are different, as they may occur in both  $2^+$  (relatively reducing conditions) and  $4^+$  (relatively oxidizing conditions) states (Panahi et al. 2000).  $\text{Ce}^{3+}$  is easily oxidized to  $\text{Ce}^{4+}$  during weathering and precipitates as  $\text{CeO}_2$  (Braun et al. 1990; Yusoff et al. 2013). As a result, the relative Ce enrichment in the upper soil (oxidizing conditions) causes a positive Ce anomaly in the TML profile, and, with less Ce leaching from this zone to the bottom of the profile, the subsoil shows a negative Ce anomaly. Eu is also redox-sensitive; the ionic radii of  $\text{Eu}^{2+}$  (1.25 Å) closely resembles  $\text{Sr}^{2+}$  (1.18 Å), so that under reducing conditions, the  $\text{Eu}^{2+}$  ion will likely display similar geochemical behavior to  $\text{Sr}^{2+}$  (Krupka and Serne 2002). However, Fig. 8a shows a negative correlation between them, and the  $\delta\text{Eu}$  value increased with weathering intensity, shown by  $\text{Rb/Sr}$  (Fig. 8b). It is commonly

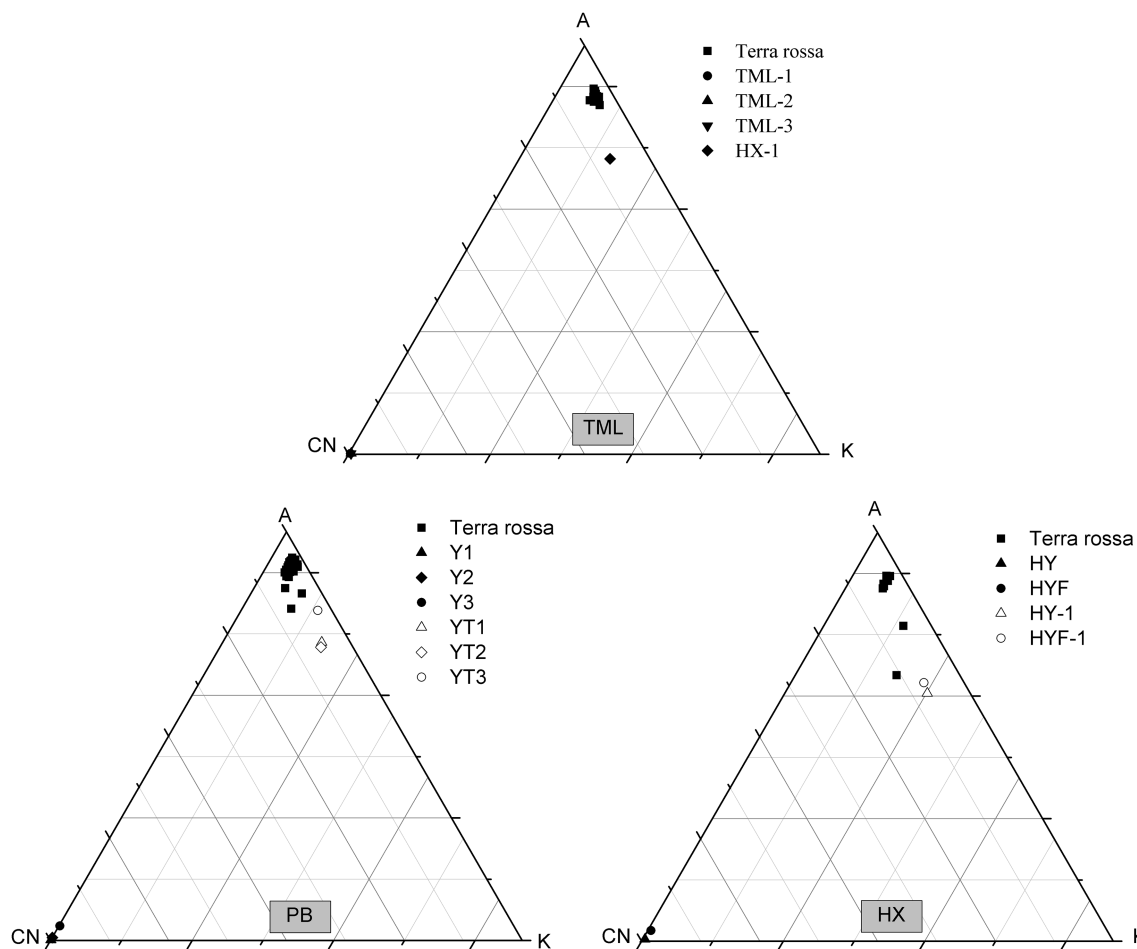


**Fig. 5** Ternary diagrams of  $\text{Al}_2\text{O}_3$  (A),  $\text{CaO} + \text{Na}_2\text{O}$  (CN) and  $\text{K}_2\text{O}$  (K) from samples of different profiles. HY and HYF denote limestone and its rock powder, respectively, and HY-1 and HYF-1 denote the acid insoluble residues from those samples. YT1, YT2 and YT3 denote the acid insoluble residues from samples Y1, Y2 and Y3, respectively. The Huaxi (HX) and Pingba (PB) data are from Sun et al. (2002b) and Ji et al. (2004a); the HX profile developed on limestone, while the others developed on dolostone

believed that a negative Eu anomaly in silicate weathered crust can be attributed to plagioclase fractionation (Aubert et al. 2001; Malpas et al. 2001), while the variations of  $\delta\text{Eu}$  in lateritic soil covering carbonate rocks is not consistent with the concentration of plagioclase (Wei et al. 2014). Table 3 shows a negative Eu anomaly in the whole profile and potential sources, but there is a lack of large amplitude variation in the soil layer with a range of  $\delta\text{Eu}$  from 0.60–0.70 (Table 3). It is possible that the redox conditions of the parent rock may have influenced Eu.

Figure 9 shows the cross plots of  $\text{Ce}/\text{Ce}^*$  and  $\text{La}_N/\text{Yb}_N$  from Pingba (PB1, PB2), Huchao (HC) and TML profiles that developed on the same strata (Anshun Formation). The bedrock from PB1 (Li et al. 1998), HC (Sun 2002) and TML show the same composition, but PB2 (Sun et al. 2002a) is different; the soil shows different distributions in each of the profiles. The lowermost soil samples (TML4–8) concentrate beside the bedrock samples (TML1–3),

whereas the uppermost soil shows different characteristics different. However, these characteristics were not found in previously studied profiles (Fig. 9). The results reflect the heterogeneity of bedrock and the different formation processes of terra rossa.

## 4.2 The inherent relationship between terra rossa and the overlying strata

### 4.2.1 Estimating the laterite-forming capacity of a possible source

The content of acid insoluble residues of the Anshun Formation is 0.68 % in the studied profile. According to the formula provided by Yuan and Cai (1988), the thickness (H) of a carbonate rock that dissolved to form a terra rossa can be estimated based on the content of acid insoluble residues in the bedrock:

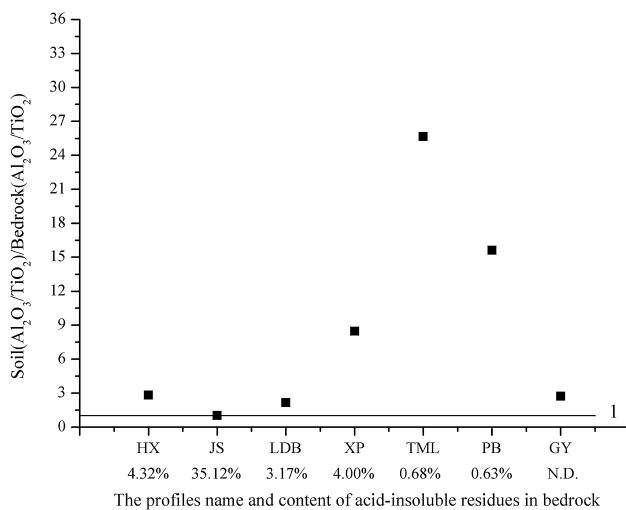


**Fig. 6** The ratio of soil( $\text{Al}_2\text{O}_3/\text{TiO}_2$ )/bedrock( $\text{Al}_2\text{O}_3/\text{TiO}_2$ ). The ratio  $\text{Al}_2\text{O}_3/\text{TiO}_2$  in terra rossa represents the soil average. Huaxi (HX), Jishou (JS), Pingba (PB) and Xinpu (XP) data are from Sun et al. (2002b), Wang et al. (2002), Ji et al. (2000) and Ji et al. (2004a), and Longdongbao (LDB) and Guiyang (GY) data are from Zhou et al. (2005), Feng et al. (2007) and Li et al. (1991). ND no data

$$H = (T \times M \times A_1 \times G_1) / (N \times A_2 \times G_2), \quad (1)$$

where  $T$  is soil thickness (terra rossa thickness in the TML profile is 8 m),  $M$  is the total amount (%) of dissolution residue in the soil (Wang et al. 1999),  $A_1$  (distribution area of the relict soil) is assumed to be  $1 \text{ km}^2$ ,  $G_1$  (soil density) is  $1.9 \text{ t/m}^3$  (Yuan and Cai 1988),  $N$  is the total amount of dissolution residue of carbonate rock deduced from the leaching experiment,  $A_2$  (distribution area of the dissolved carbonate rock) is assumed to be  $1 \text{ km}^2$ , and  $G_2$  is the density of carbonate rock ( $\text{t/m}^3$ ) and dolomite ( $2.85 \text{ t/m}^3$ ) (Wang et al. 1999).

Solving for Eq. 1 indicates that a 674.98-m-thick Anshun Formation dolomite could be dissolved to form an

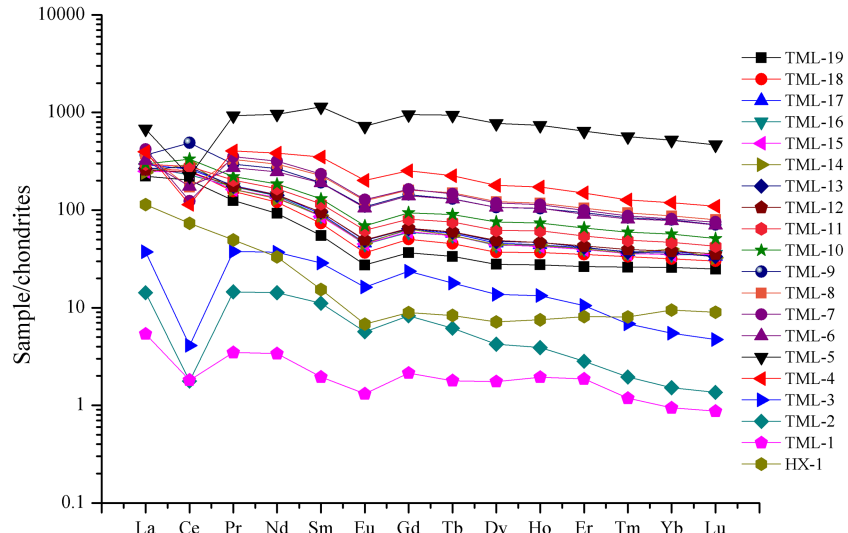
8-m soil thickness. However, the thickness of the Anshun Formation only ranges from 50–301 m in the study area (1:200,000 regional geological map, 1977). Therefore, an 8-m-thick terra rossa could not form from the acid insoluble residues in the bedrock alone.

The major geological structure in the study area is the Guiyang syncline. According to the stratigraphic relationship, the exposed Anshun Formation in the syncline wings could be associated with the weathering and erosion of the overlying strata. Thus, the laterite-forming capacity of the strata covering the Anshun Formation was estimated. Table 4 lists the results of different calculations without considering erosion or compaction. Clearly, plenty of weathered residual material remained to form the terra rossa, as only the Ziliujing Formation formed soil more than 200-m-thick after the entire stratum weathered. Table 5 shows the major element contents in the strata overlaying the Anshun Formation. As shown in Table 5, clastic rock and acid insoluble substances have the same composition in terms of  $\text{Al}_2\text{O}_3$ ,  $\text{SiO}_2$ ,  $\text{Fe}_2\text{O}_3$  and LOI, which accounts for 86 w%–99 w%. These were also the main components of the terra rossa (Table 1) and thus, the overlying strata could provide a considerable amount of material to form the terra rossa in the studied profile. Furthermore, Al and Fe are less mobile during chemical weathering.  $\text{Al}_2\text{O}_3$  and  $\text{Fe}_2\text{O}_3$  show significant positive correlations to the weathering residue and potential parent materials (Fig. 10), reflecting the enrichment of  $\text{Al}_2\text{O}_3$  and  $\text{Fe}_2\text{O}_3$  from rocks to terra rossa.

#### 4.2.2 Evidence from the trace element distribution patterns

Nb and Ta are stable during laterization, alteration and bauxitization (Gong et al. 2011). If the TML profiles showed in situ crustal weathering, the Nb/Ta of the bottom

**Fig. 7** Chondrite-normalized REE spider diagrams



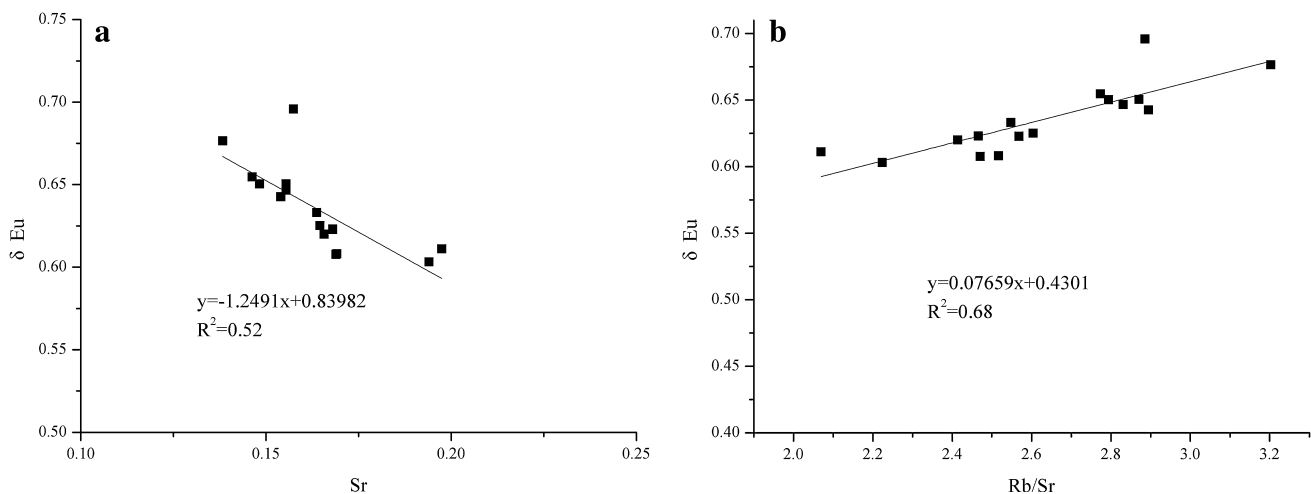


**Fig. 8** **a** Sr versus  $\delta\text{Eu}$  and **b** Rb/Sr versus  $\delta\text{Eu}$  of samples from the TML profile

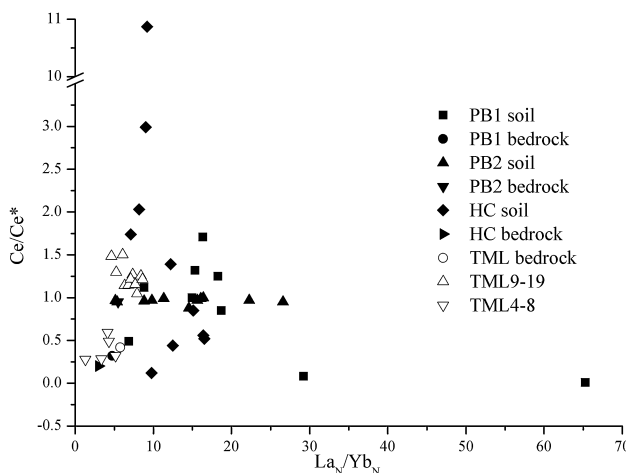


**Fig. 9** Cross plots of Ce/Ce\* and La<sub>N</sub>/Yb<sub>N</sub> for terra rossa samples and the underlying Anshun Formation dolomite. The Pingba (PB1, PB2) and Huchao (HC) data are from Li et al. (1998), Sun (2002, 2002a)

soil in the profiles should be close to that of acid insoluble residues from bedrock. However, the bottom soils were not close to the acid insoluble residues from the Anshun Formation (sample HX-1), suggesting that the studied profiles do not possess the characteristics of in situ weathering (Fig. 11). The soil samples show a dispersed distribution rather than a concentration in a small region, indicating that more than one source contributed to the formation of the terra rossa. According to a correlation analysis between CR1–7, T<sub>2g</sub>-1, T<sub>2yl</sub>-1, HX-1 and the terra rossa, their correlation coefficients ( $R^2$ ) were higher than 0.90, and the soils distributed between acid insoluble residues (T<sub>2g</sub>-1, T<sub>2yl</sub>-1, HX-1) and clastic rocks (CR1–7), suggesting that the formation of the terra rossa in the TML profiles probably had at least four sources.

The abundance of immobile trace elements (e.g., Sc, Th, La and Zr), when displayed on ternary diagrams, is a powerful tool for identifying distinct provenance types and tectonic settings (Bauluz et al. 2000; Purevjav and Roser 2013). The same approach can be used for the parent materials of terra rossa. (Muhs and Budahn 2009) stated that volcanic ash and eolian dust are parent materials for terra rossa in northern Jamaica. In Fig. 12, almost all of the terra rossa points are distributed between acid insoluble residues from carbonate and clastic rocks, whereas the terra rossa samples from the TML profile were closer to the Erqiao + Sanqiao and Ziliujing Formations (CR1–7). These results suggest that the weathering of clastic rocks may be the main source contributing to the terra rossa. Sc–Th-Ta can also be used to identify the parent material of the terra rossa in the studied profiles, which also indicates that many soils present the mixed characteristic of acid insoluble residues from carbonate rocks and clastic rocks (CR).

#### 4.2.3 Evidence from REEs

The topsoil and subsoil show different REE distribution patterns. However, the shape of the chondrite-normalized REE patterns inclines towards the right in the whole profile, indicating LREE enrichment (Fig. 7) and a negative Eu anomaly in the terra rossa (Table 3). These characteristics show the same composition as the potential source material (Fig. 13), but with differences in REE content. Furthermore, the ΣREE in the potential parent materials (CR1–7, T<sub>2g</sub>-1 and T<sub>2yl</sub>-1) ranges from 32.89 ppm to 195.14 ppm. The content is higher than the underlying bedrock and their insoluble residues (Table 3), so that the ΣREE could be gradually enriched with weathering.

**Table 4** The laterite-forming capacity estimate for the overlying strata of the Anshun Formation

Stratigraphic	Symbol	Strata age	Strata thickness	Lithology	Reference data	The potential thickness of soil
Ziliujing	Jz1	Jurassic	1084–1333 m	Clastic rocks	20 % laterite-forming capacity <sup>a</sup>	216.8–246.6 m
Erqiao + Sanqiao	T <sub>3</sub> e + s	Triassic	93–208 m		30 % laterite-forming capacity <sup>a</sup>	27.9–62.4 m
Yangliujing	T <sub>2</sub> yl		60–620 m	Carbonate rocks	5.3 % <sup>b</sup>	3.18–32.86 m
Guanling	T <sub>2</sub> g		160–372 m	rocks	0.19 % <sup>b</sup>	0.30–0.71 m

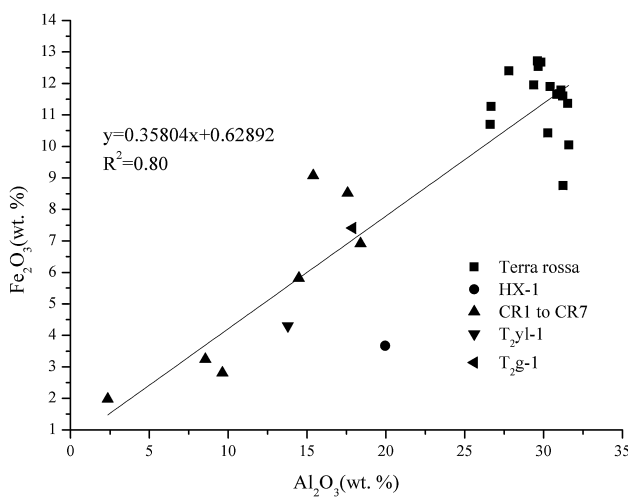
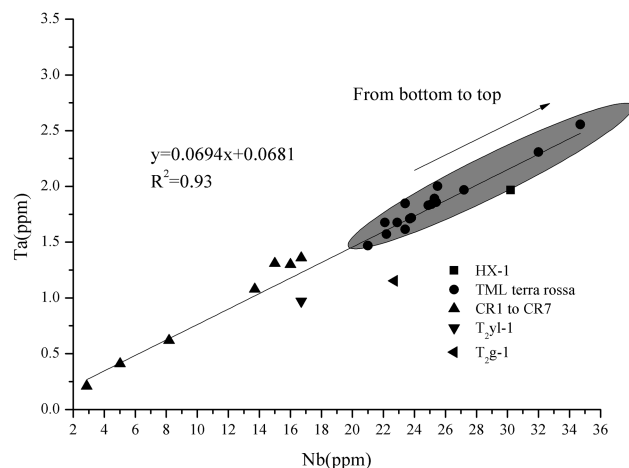
<sup>a</sup> The laterite-forming capacity is an empirical value that indicates how much residue could remain in situ to form soil after the weathering of the strata. The data were obtained from (Yang and Wei 2008)

<sup>b</sup> The content of acid insoluble residues

**Table 5** Major element contents of bulk samples from overlying strata (w%)

Rock samples <sup>a</sup>	SiO <sub>2</sub>	Al <sub>2</sub> O <sub>3</sub>	TFe <sub>2</sub> O <sub>3</sub>	CaO	MgO	K <sub>2</sub> O	Na <sub>2</sub> O	MnO	TiO <sub>2</sub>	P <sub>2</sub> O <sub>5</sub>	LOI	Total
CR-1	82.48	9.63	2.81	0.18	0.35	1.60	0.10	0.01	0.27	0.06	2.49	99.97
CR-2	50.53	15.39	9.08	9.17	2.29	3.25	0.17	0.06	0.66	0.11	12.55	103.26
CR-3	61.16	18.39	6.91	0.07	1.28	3.58	0.17	0.03	0.80	0.09	7.50	99.98
CR-4	84.47	8.56	3.24	0.06	0.06	0.32	0.05	0.01	0.50	0.05	2.50	99.81
CR-5	59.09	17.57	8.52	0.46	1.15	2.11	0.11	0.05	0.97	0.08	10.12	100.23
CR-6	53.54	14.48	5.82	7.69	2.07	2.44	0.15	0.08	0.69	0.13	13.01	100.10
CR-7	94.11	2.36	1.98	0.12	0.07	0.18	0.05	0.02	0.24	0.04	0.70	99.87
T <sub>2</sub> yl	3.45	0.79	0.28	31.70	18.79	0.26	0.26	0.02	0.04	0.04	44.86	100.49
T <sub>2</sub> g	0.10	0.03	–	49.38	5.94	0.02	–	0.002	0.01	0.02	44.34	99.84
T <sub>2</sub> yl-1	66.16	13.78	4.30	0.11	1.51	3.66	0.04	0.01	0.73	0.06	8.22	98.58
T <sub>2</sub> g-1	52.93	17.89	7.41	0.77	1.92	4.40	0.79	0.02	0.91	0.07	11.40	98.51

<sup>a</sup> CR-1 to CR-7 represent clastic rock collected from the Erqiao + Sanqiao and Ziliujing Formations. T<sub>2</sub>yl and T<sub>2</sub>g denote the Yangliujing and Guanling Formation carbonate rocks, respectively, and T<sub>2</sub>yl-1 and T<sub>2</sub>g-1 denote the acid-insoluble residues from samples T<sub>2</sub>yl and T<sub>2</sub>g, respectively. The symbol “–” indicates the content is under the test limit

**Fig. 10** Distribution of Fe<sub>2</sub>O<sub>3</sub> versus Al<sub>2</sub>O<sub>3</sub>. Significant correlations**Fig. 11** Distribution scatter plot of Nb and Ta in samples from the TML profile

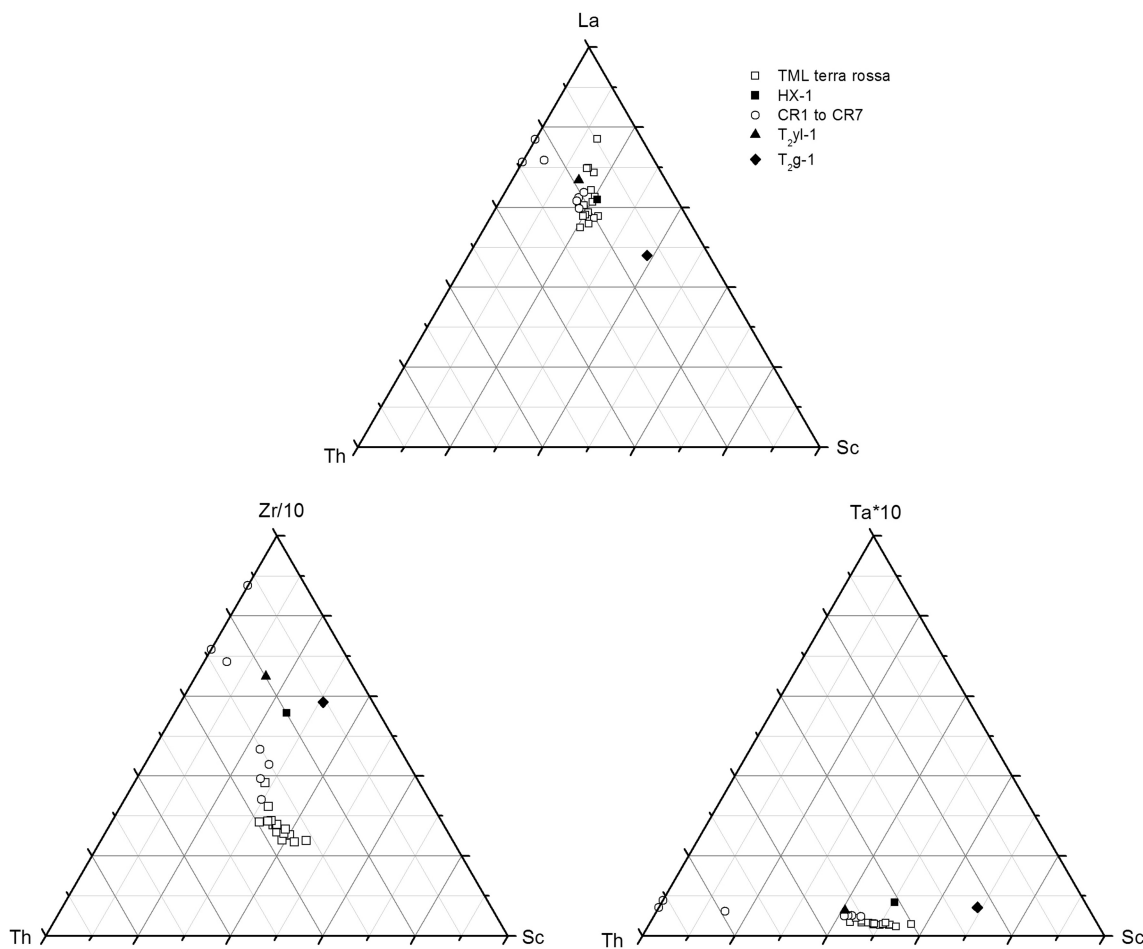


**Fig. 12** Ternary diagrams for Sc, Th, Zr, and Ta showing the compositions of the TML profile and potential parent material

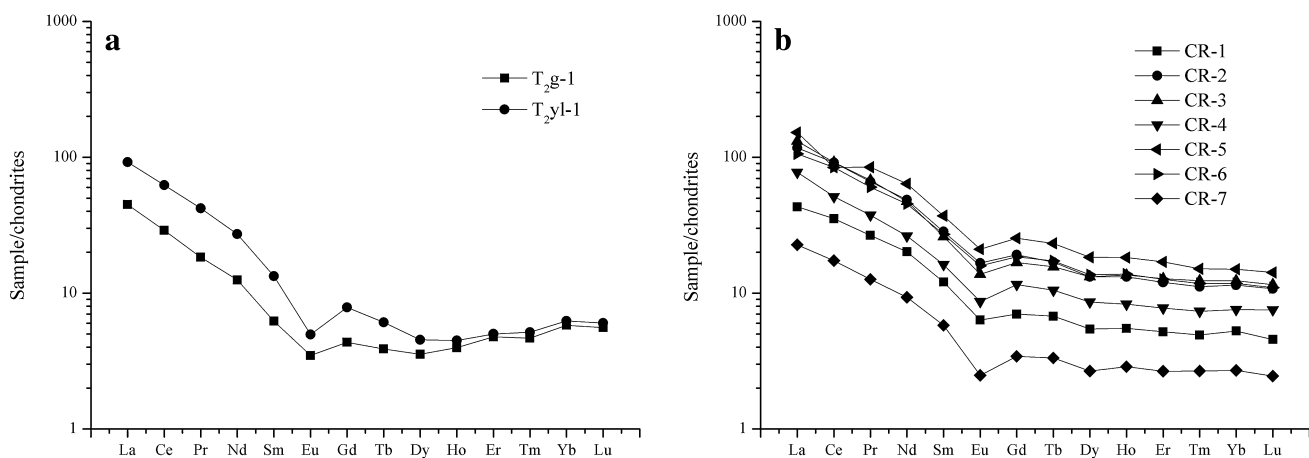


**Fig. 13** Chondrite-normalized REE spider diagrams for the topsoil in the studied profiles and potential parent material

The  $\text{La}_N/\text{Yb}_N$  ratio indicates HREE depletion and, thus, lower  $\text{La}_N/\text{Yb}_N$  reflects HREE enrichment. Because the REE compositions are different,  $\text{Eu}/\text{Eu}^*$  versus  $\text{Gd}_N/\text{Yb}_N$  was used to study the origin of the sediments, bauxite

deposits, terra rossa and the loess sources (McLennan 1989; Sun et al. 2002b; Muhs and Budahn 2009; Wei et al. 2013). Cross plots of  $\text{Eu}/\text{Eu}^*$  and  $\text{Gd}_N/\text{Yb}_N$  (Fig. 14) show that there is some overlap between the terra rossa and

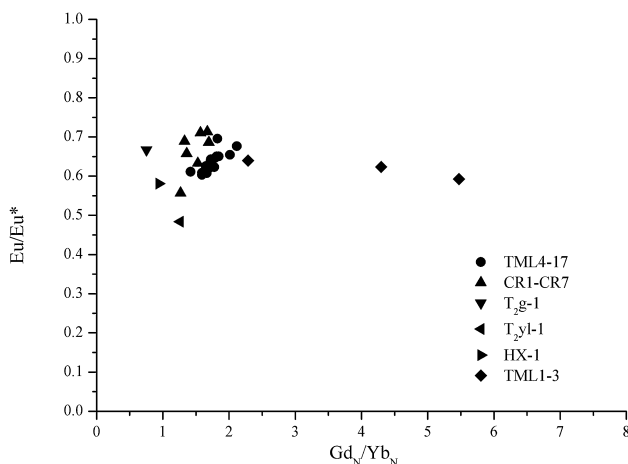


**Fig. 14** Cross plots of  $\text{Eu}/\text{Eu}^*$  values and  $\text{Gd}_N/\text{Yb}_N$  of the TML profile and potential source material

clastic rocks (CR1–7) and that all of the soil samples are separated from the bedrock and its acid insoluble residues (TML1–3, HX-1). The terra rossa falls between the bedrock and potential parent materials (CR1–7,  $T_{2g}$ -1,  $T_{2yl}$ -1). This indicates that the terra rossa in the study area probably incorporates material from the overlying strata.

## 5 Conclusions

This study investigated the geochemical characteristics of element distribution and parent materials of the Tongmuling profile, including the overlying strata covering the bedrock during geological history, and developed on the Triassic dolomite of the Yunnan–Guizhou Plateau. The results indicated that the TML profile was not formed from *in situ* weathering. While the insoluble bedrock residue contributed to the terra rossa formation, the major, trace and rare earth element results suggested that external material affected its genesis. In particular, overlying strata, deposited over time, likely provided parent material for the genesis of terra rossa.

**Acknowledgments** We thank the two anonymous reviewers for their critical comments on the manuscript. This work was financially supported by the National Basic Research Program of China (Grants No. 2006CB403202).

## References

- Ahmad N, Jones RL, Beavers AH (1966) Genesis, mineralogy and related properties of West Indian Soils: I. Bauxitic soils of Jamaica. *Soil Sci Soc Am J* 30:719–722
- Aubert D, Stille P, Probst A (2001) REE fractionation during granite weathering and removal by waters and suspended loads: Sr and Nd isotopic evidence. *Geochim Cosmochim Acta* 65:387–406
- Bauluz B, Mayayo MJ, Fernandez-Nieto C, Gonzalez Lopez JM (2000) Geochemistry of Precambrian and Paleozoic siliciclastic rocks from the Iberian Range (NE Spain): implications for source-area weathering, sorting, provenance, and tectonic setting. *Chemical Geology* 168:135–150
- Boynton WV (1984) Cosmochemistry of the rare earth elements: meteorite studies. In: Henderson P (ed) Rare earth element geochemistry, vol 2. Elsevier, Amsterdam, pp 63–114
- Braun J-J, Pagel M, Muller J-P, Bilong P, Michard A, Guillet B (1990) Cerium anomalies in lateritic profiles. *Geochim Cosmochim Acta* 54:781–795
- Bronger A, Ensling J, Guetlich P, Spiering H (1983) Rubification of terra rossa in Slovakia: a Mössbauer effect study. *Clays Clay Miner* 31:269–276
- Bugge B, Glaser B, Hambach U, Gerasimenko N, Marković S (2011) An evaluation of geochemical weathering indices in loess-paleosol studies. *Quatern Int* 240:12–21
- Cooke MJ, Stern LA, Banner JL, Mack LE (2007) Evidence for the silicate source of relict soils on the Edwards Plateau, central Texas. *Quatern Res* 67:275–285
- Cui Z, Li D, Liu G, Feng J, Zhang W (2001) Characteristics and planation surface formation environment of the red weathering crust in Hunan, Guangxi, Yunnan, Guizhou and Tibet. *Sci China* 44(1):162–175
- Delgado R, Martin-Garcia JM, Oyonarte C, Delgado G (2003) Genesis of the terra rossae of the Sierra Gádor (Andalusia, Spain). *Eur J Soil Sci* 54:1–16
- Duddy LR (1980) Redistribution and fractionation of rare-earth and other elements in a weathering profile. *Chem Geol* 30:363–381
- Durn G (2003) Terra Rossa in the Mediterranean Region: parent Materials, Composition and Origin. *Geol Croat* 56:83–100
- Durn G, Ottner F, Slovenec D (1999) Mineralogical and geochemical indicators of the polygenetic nature of terra rossa in Istria, Croatia. *Geoderma* 91:125–150
- Durn G, Aljinović D, Crnjaković M, Lugović B, vers Detroit A (2007) Heavy and light mineral fractions indicate polygenesis of extensive terra rossa soils in Istria, Croatia. In: Mange MA, Wright DT (eds) Developments in sedimentology, vol 58. Elsevier, Amsterdam, pp 701–737
- Feng Z, Wang S, Liu X, Luo W (2007) Micro-area transportation of residues: style of forming the red weathering crusts of carbonate rocks. *Acta Geol Sin* 81:127–138 (in Chinese)
- Feng J, Zhu L, Cui Z (2009) Quartz features constrain the origin of terra rossa over dolomite on the Yunnan–Guizhou Plateau, China. *J Asian Earth Sci* 36:156–167
- Gong Q, Deng J, Yang L, Zhang J, Wang Q, Zhang G (2011) Behavior of major and trace elements during weathering of sericite-quartz schist. *J Asian Earth Sci* 42:1–13
- Hill IG, Worden RH, Meighan IG (2000) Yttrium: the immobility-mobility transition during basaltic weathering. *Geology* 28:923–926
- Huang Z (1996) The red weathering crust in southern China (in Chinese). Ocean Press, Beijing
- Ji H, Ouyang Z, Wang S, Zhou D (2000) Element geochemistry of weathering profile of dolomite and its implications for the average chemical composition of the upper-continental crust—Case studies from the Xinpu profile, northern Guizhou Province, China. *Sci China* 41:23–35
- Ji H, Wang S, Ouyang Z, Zhang S, Sun C, Liu X, Zhou D (2004a) Geochemistry of red residua underlying dolomites in karst terrains of Yunnan–Guizhou Plateau I. The formation of the Pingba profile. *Chem Geol* 203:1–27
- Ji H, Wang S, Ouyang Z, Zhang S, Sun C, Liu X, Zhou D (2004b) Geochemistry of red residual underlying dolomites in karst terrains of Yunnan–Guizhou Plateau II. The mobility of rare earth elements during weathering. *Chem Geol* 203:29–50

- Jiang Y, Wu Y, Grovers C, Yuan D, Kambesis P (2009) Natural and anthropogenic factors affecting the groundwater quality in the Nandong karst underground river system in Yunan, China. *J Contam Hydrol* 109:49–61
- Krupka KM, Serne RJ (2002) Geochemical factors affecting the behavior of antimony, cobalt, europium, technetium, and uranium in vadose sediments. Pacific Northwest National Laboratory, Richland
- Laveuf C, Cornu S (2009) A review on the potentiality of Rare Earth Elements to trace pedogenetic processes. *Geoderma* 154:1–12
- Li J, Wang C, Fan T (1991) Weathering crust of carbonate rocks and process of karst earth formation (in Chinese). *Carsologica Sin* 10:29–38
- Li J, Zhu L, Chen J (1998) Rare earth element distribution in weathering cursts of carbonate rocks, Guizhou Province (in Chinese). *Carsologica Sin* 17:15–24
- Liu W-J, Liu C-Q, Zhao Z-Q, Xu Z-F, Liang C-S, L-b Li, Feng J-Y (2013) Elemental and strontium isotopic geochemistry of the soil profiles developed on limestone and sandstone in karstic terrain on Yunnan-Guizhou Plateau, China: implications for chemical weathering and parent materials. *J Asian Earth Sci* 67–68:138–152
- Lucke B, Kemnitz H, Bäumler R, Schmidt M (2014) Red Mediterranean Soils in Jordan: new insights in their origin, genesis, and role as environmental archives. *Catena* 112:4–24
- Malpas J, Duzgoren-Aydin NS, Aydin A (2001) Behaviour of chemical elements during weathering of pyroclastic rocks, Hong Kong. *Environ Int* 26:359–368
- McLennan SM (1989) Rare earth elements in sedimentary rocks; influence of provenance and sedimentary processes. *Rev Miner Geochem* 21:169–200
- Mee AC, Bestland EA, Spooner NA (2004) Age and origin of Terra Rossa soils in the Coonawarra area of South Australia. *Geomorphology* 58:1–25
- Merino E, Banerjee A (2008) Terra rossa genesis, implications for karst, and eolian dust: a geodynamic thread. *J Geol* 116:62–75
- Merino E, Banerjee A, Dworkin S (2006) Dust, terra rossa, replacement, and karst: serendipitous geodynamics in the critical zone. *Geochim Cosmochim Acta* 70:A416
- Muhs DR, Budahn JR (2009) Geochemical evidence for African dust and volcanic ash inputs to terra rossa soils on carbonate reef terraces, northern Jamaica, West Indies. *Quatern Int* 196:13–35
- Muhs DR, Bush CA, Stewart KC, Rowland TR, Crittenden RC (1990) Geochemical evidence of Saharan dust parent material for soils developed on Quaternary limestones of Caribbean and western Atlantic islands. *Quatern Res* 33:157–177
- Nesbitt HW (1979) Mobility and fractionation of rare earth elements during weathering of a granodiorite. *Nature* 279:206–210
- Nesbitt HW, Markovics G (1997) Weathering of granodioritic crust, long-term storage of elements in weathering profiles, and petrogenesis of siliciclastic sediments. *Geochim Cosmochim Acta* 61:1653–1670
- Nesbitt HW, Young GM (1982) Early Proterozoic climates and plate motions inferred from major element chemistry of lutites. *Nature* 229:715–717
- Nesbitt HW, Young GM (1989) Formation and diagenesis of weathering profiles. *J Geol* 97:129–147
- Nesbitt HW, Markovics G, Price RC (1980) Chemical processes affecting alkalis and alkaline earths during continental weathering. *Geochim Cosmochim Acta* 44:1659–1666
- Olson CG, Ruhe RV, Mausbach MJ (1980) The terra rossa limestone contact phenomena in karst, Southern Indiana. *Soil Sci Soc Am J* 44:1075–1079
- Panahi A, Young GM, Rainbird RH (2000) Behavior of major and trace elements (including REE) during Paleoproterozoic pedogenesis and diagenetic alteration of an Archean granite near Ville Marie, Québec, Canada. *Geochim Cosmochim Acta* 64:2199–2220
- Plank T, Langmuir CH (1998) The chemical composition of subducting sediment and its consequences for the crust and mantle. *Chem Geol* 145:325–394
- Purevjav N, Roser B (2013) Geochemistry of Silurian-Carboniferous sedimentary rocks of the Ulaanbaatar terrane, Hangay-Hentey belt, central Mongolia: provenance, paleoweathering, tectonic setting, and relationship with the neighbouring Tsetserleg terrane. *Chem Erde* 73:481–493
- Rye R, Holland HD (1998) Paleosols and the evolution of atmospheric oxygen: a critical review. *Am J Sci* 298:621–672
- Sandler A, Meunier A, Velde B (2015) Mineralogical and chemical variability of mountain red/brown Mediterranean soils. *Geoderma* 239–240:156–167
- Sun C (2002) Soil material source and rare earth elements chemistry in the carbonate rock weathering profiles in Guizhou Province. Chinese Academy of Sciences, Beijing (in Chinese)
- Sun C, Wang S, Ji H (2002a) Formation mechanism of the superhigh concentration of REE and the strong negative Ce anomalies in the carbonate rock weathering profiles in Guizhou Province, China (in Chinese). *Geochimica* 31:119–128
- Sun C, Wang S, Liu X, Feng Z (2002b) Geochemical characteristics and formation mechanism of rock-soil interface in limestone weathering crust at Huaxi, Guizhou Province (in Chinese). *Acta Mineralogica Sinica* 22:126–132
- Taylor SR, McLennan SM (1985) The continental crust: Its composition and evolution. Blackwell Scientific Publications, Oxford
- Team GPGS (1995) Dictionary of Stratigraphic Terms of Guizhou (in Chinese). Guizhou Science and Technology Press, Guiyang
- Wang S, Ji H, Ouyang Z, Zhou D, Zhen L, Li T (1999) Preliminary study on weathering and pedogenesis of carbonate rock. *Sci China* 42:572–581
- Wang S, Sun C, Feng Z, Liu X (2002) Mineralogical and geochemical characteristics of the limestone weathering profile in Jishou, western Hunan Province, China (in Chinese). *Acta Miner Sin* 22:19–29
- Wei X, Ji H, Li D, Zhang F, Wang S (2013) Material source analysis and element geochemical research about two types of representative bauxite deposits and terra rossa in western Guangxi, southern China. *J Geochem Explor* 133:68–87
- Wei X, Ji H, Wang S, Chu H, Song C (2014) The formation of representative lateritic weathering covers in south-central Guangxi (southern China). *Catena* 118:55–72
- Wu P, Tang C, Zhu L, Liu C, Cha X, Tao X (2009) Hydrogeochemical characteristics of surface water and groundwater in the karst basin, southwest China. *Hydrol Process* 23:2012–2022
- Yang R, Wei H (2008) Using lithologic characteristics and strata thicknesses in karst region to estimate laterite-forming capacity:a case study for Triassic-Jurassic sediments in Jingyang district, Guiyang City, Guizhou Province (in Chinese). *Geol J China Univ* 14:82–89
- Young GM, Nesbitt HW (1998) Processes controlling the distribution of Ti and Al in weathering profiles, siliciclastic sediments and sedimentary rocks. *J Sediment Res* 68:448–455
- Yuan D (1992) Karst in southwest China and its comparison with karst in north China (in Chinese). *Quatern Sci* 4:352–361
- Yuan D, Cai G (1988) Karst Environment (in Chinese). Chongqing Press, Chongqing

- Yusoff ZM, Ngwenya BT, Parsons I (2013) Mobility and fractionation of REEs during deep weathering of geochemically contrasting granites in a tropical setting, Malaysia. *Chem Geol* 349–350:71–86
- Zhou D, Wang S, Liu X (2005) Study on geochemical processes in limestone soil profiles. *Earth Environ* 33:31–38 (in Chinese)
- Zhu L, Li J (2002) Mechanism of weathering pedogenesis of carbonate rocks: I. Mineralogical and micro-textural evidence. *Chin J Geochem* 21:334–339
- Zhu L, He S, Li J (2008) Weathering-pedogenesis of carbonate rocks and its environmental effects in subtropical region. *Acta Geol Sin* 88:982–993